UNIVERSITY OF
Southampton
Institute of Sound and
Vibration Research

ISVR Technical Report

Dynamics of Gas Bubbles in Viscoelastic Media Accounting for High Amplitude Pulses and Second Harmonic Emissions

H. Dogan and T.G. Leighton

ISVR Technical Report No 337

December 2015

SCIENTIFIC PUBLICATIONS BY THE ISVR

Technical Reports are published to promote timely dissemination of research results by ISVR personnel. This medium permits more detailed presentation than is usually acceptable for scientific journals. Responsibility for both the content and any opinions expressed rests entirely with the author(s).

Technical Memoranda are produced to enable the early or preliminary release of information by ISVR personnel where such release is deemed to the appropriate. Information contained in these memoranda may be incomplete, or form part of a continuing programme; this should be borne in mind when using or quoting from these documents.

Contract Reports are produced to record the results of scientific work carried out for sponsors, under contract. The ISVR treats these reports as confidential to sponsors and does not make them available for general circulation. Individual sponsors may, however, authorize subsequent release of the material.

COPYRIGHT NOTICE

(c) ISVR University of Southampton All rights reserved.

ISVR authorises you to view and download the Materials at this Web site ("Site") only for your personal, non-commercial use. This authorization is not a transfer of title in the Materials and copies of the Materials and is subject to the following restrictions: 1) you must retain, on all copies of the Materials downloaded, all copyright and other proprietary notices contained in the Materials; 2) you may not modify the Materials in any way or reproduce or publicly display, perform, or distribute or otherwise use them for any public or commercial purpose; and 3) you must not transfer the Materials to any other person unless you give them notice of, and they agree to accept, the obligations arising under these terms and conditions of use. You agree to abide by all additional restrictions displayed on the Site as it may be updated from time to time. This Site, including all Materials, is protected by worldwide copyright laws and treaty provisions. You agree to comply with all copyright laws worldwide in your use of this Site and to prevent any unauthorised copying of the Materials.

UNIVERSITY OF SOUTHAMPTON

INSTITUTE OF SOUND AND VIBRATION RESEARCH

ACOUSTICS GROUP

Dynamics of Gas Bubbles in Viscoelastic Media Accounting for High Amplitude Pulses and Second Harmonic Emissions

by

H. Dogan and T. G. Leighton

ISVR Technical Report No. 337

December 2015

Authorized for issue by
Professor P F Joseph

© Institute of Sound and Vibration Research

ACKNOWLEDGEMENTS

This work is funded by National Environment Research Council UK (Grant number NE/J022403/1, Principal Investigator Prof T.G. Leighton).

CONTENTS

1 Introduction 4
2 Theory 5
2.1 Matching asymptotic solutions 7
2.2 Evaluating stress components 9
2.3 Bubble dynamics 9
2.4 Analytical solutions 11
2.5 Harmonic expansions 14
2.6 Scattering Cross Sections 16
3 Results 17
3.1 Reproduction of results for soft tissue (Yang and Church 2004) 17
3.1.1 Resonance frequency 17
3.1.2 Linear damping coefficients 18
3.1.3 Scattering cross sections 21
3.1.4 Radius-time curves (Numerical Results) 24
3.1.5 Second harmonic emissions 26
3.2 Application of the model to sediments 27
3.2.1 Linear damping coefficients 28
3.2.2 Scattering cross section 32
4 Discussions and conclusions 34

Dynamics of gas bubbles in viscoelastic media accounting for high amplitude pulses and second harmonic emissions

Abstract

More than three decades ago, Anderson and Hampton [1980a, 1980b] (A&H) presented the theories for wave propagation in gassy water, saturated sediments and gassy sediments in their two-part review, which has been cited by many researchers in the geoacoustics and underwater acoustics areas. They gave an empirical formulation based on the theory of Spitzer [1943] for the wave propagation in gassy water by adapting that for a viscoelastic, lossy medium, though without providing a detailed derivation. Following Leighton [2007], this paper presents a theory based on non-stationary nonlinear dynamics of spherical gas bubbles and extends that 2007 paper to include liquid compressibility and thermal damping effects. The paper then shows how that nonlinear formulation can be reduced to the linear limit, and from this it derives the expressions for the damping coefficients, the scattering cross section, the speed of sound and the attenuation, and compares these with the A&H theory. The current formulation has certain advantages over A&H theory such as implementing an energy conservation based, nonlinear model for the gas pressure inside the bubble, having no sign ambiguity for the speed of sound formula (which is important when estimating the bubble void fraction in marine sediments) and correcting the ambiguity on the expression for scattering cross section, as identified in the recent work of Ainslie and Leighton [2011].

1 Introduction

Extensive distributions of seafloor methane gas and hydrates have been detected at many locations around the world by geological surveys (Best et al. [2006]). The presence of gas and its effects on the physical properties of the marine sediment are of interest for several applications, including drilling operations, construction of seafloor structures, and environmental considerations such as global warming, climate change and the slope stability of the sediments (Best et al. [2004]). Furthermore, as part of future Carbon Capture and Storage (CCS) projects, which aim at reducing atmospheric greenhouse effects, the long term acoustic monitoring of greenhouse gases' seepage in sub-seafloor reservoirs will be crucial. As such, the acoustic estimation models and tools, either via remote sensing or in laboratory conditions, require in-depth and accurate theoretical framework for the wave propagation in gassy mediums. The latter currently relies on the benchmark work of Anderson and Hampton [1980a, 1980b] (will be abbreviated as A&H theory hereafter) which presented an extensive review of the theories for wave propagation in gassy water, saturated sediments and gassy sediments up until their publication date. Given the amount of the subsequent research in geoacoustics, it is surprising that neither the fundamentals underlying their theory are questioned nor the experimental results are compared with the predictions of the theory (few exceptions to authors' knowledge include Lyons et al. [1996], Best et al. [2004]).

The A&H theory needs to be reconsidered owing to following reasons: (i) it assumes that only linear, steady state pulsations occur, which makes the method inapplicable for high amplitude pulses and second harmonic or combination frequency signals, (ii) the expression for the viscoelastic losses are given a posteriori without a rigorous derivation, (iii) at a later date, Prosperetti et al. [1988] presented a formulation for the thermal behaviour of the gas pressure inside the bubble, which is more complete than the use of polytrophic relation A&H employed especially when bubble resonance effects are present and can be incorporated into the current problem, and (iv) the expression for the scattering cross-section, when used together with the radiation damping, involves an inconsistency in terms of frequency dependence of the expressions.

Following the pioneering work of Church [1995] on the dynamics of gas-filled, encapsulated biomedical contrast agent bubbles in an incompressible viscoelastic medium, Yang and Church [2004] presented an analysis of a similar problem assuming bubbles without a shell and taking into account the compressibility of the surrounding medium. Leighton [2007] adapts the approach of Church to study the non-stationary nonlinear

dynamics of gas bubbles in marine sediments. This report extends that prior one to include liquid compressibility and thermal damping effects, and then in the linear limit, it derives expressions for the damping coefficients, the scattering cross-section, the speed of sound and the attenuation. It differs from the work of Yang and Church [2004] by using Prosperetti's model for the thermal losses during the gas pulsations (Prosperetti et al. [1988]). It compares results based on three different models for thermal losses, the three models being: polytrophic gas state, thermal viscosity and a nonlinear formulation. Further, it removes the ambiguity in the expression for the linear scattering cross-section based on the recent work of Ainslie and Leighton [2009, 2011].

One further comment should be noted on how the above mentioned theories for acoustic propagation (the forward problem) can be used for the estimation of bubble void fraction and bubble size distribution in marine sediments (the inverse problem). As A&H theory assumes linear, steady-state pulsations of gas bubbles, it is not capable of simulating either the transient period of bubble oscillation, or the ring-down period when the insonifying field is turned off or short acoustic pulses are used. Given the current powerful state of computational sources, it is possible to use time-dependent formulations for the speed of sound and acoustic scattering and extinction cross sections (Clarke and Leighton [1998], Leighton et al. [2004]). Further the linear theory is not appropriate for high amplitude, high frequency insonification which is of increasing interest.

2 Theory

Caflish et al. [1985] presented a set of equations which describes the wave propagation in a bubbly liquid. The mass conservation equation of the model reads

$$\frac{1}{\rho c^2}\frac{\partial p}{\partial t} + \nabla \cdot \vec{v} = \frac{\partial \Gamma}{\partial t} \tag{1}$$

where $p(\vec{r},t)$, $\vec{v}(\vec{r},t)$ and $\Gamma(\vec{r},t)$ are the spatio-temporal acoustic pressure field, velocity field and void fraction of bubbles, respectively, ρ is the density and c is the sound speed in the host medium. Eq. (1) is assumed heuristically to hold also for an incompressible viscoelastic medium containing bubbles, such as marine sediments, assuming that the host medium (saturated sediment) behaves as an effective medium with equivalent bulk properties. For a mono-disperse distribution of bubbles, bubble void fraction can be expressed as

$$\Gamma(\vec{r},t) = N(\vec{r})\frac{4}{3}\pi R(\vec{r},t)^3 \tag{2}$$

with $N(\vec{r})$ being the local density of bubbles and $R(\vec{r},t)$ the bubble radius.

The conservation of momentum is given by

$$\rho\left(\frac{\partial\vec{v}}{\partial t} + (\vec{v}\cdot\nabla)\vec{v}\right) = -\nabla p + \nabla\cdot\vec{\boldsymbol{\tau}}, \tag{3}$$

where $\boldsymbol{\tau}$ denotes stress tensor. Since the surrounding medium is assumed to be incompressible, the trace of the stress tensor is zero:

$$\tau_{rr} = -\left(\tau_{\theta\theta} + \tau_{\phi\phi}\right). \tag{4}$$

For a spherically symmetric radial flow, Eq. (3) reduces to:

$$\rho\left(\frac{\partial v_r}{\partial t} + v_r\frac{\partial v_r}{\partial r}\right) = -\frac{\partial p}{\partial r} + \frac{\partial\tau_{rr}}{\partial r} + \frac{2}{r}[\tau_{rr} - \tau_{\theta\theta}] \tag{5}$$

where v_r is the radial velocity. Note that $\tau_{\theta\theta} = \tau_{\phi\phi}$ for a spherically symmetric flow. In order to complete the above problem, the boundary and initial conditions are prescribed as follows:

$$p(R,t) - \tau_{rr}(R,t) = p_{\mathrm{g}} - \frac{2\sigma}{R} \qquad \text{at } r = R,$$

$$p = p_0 \qquad \text{at } r = \infty,$$

$$R = R_0,\ \ \dot{R} = 0 \qquad \text{at } t = 0,$$

where p_{g} is the gas pressure inside the bubble, σ indicates the surface tension, $p_0$is pressure in the far field in the undisturbed state, R_0 is the equilibrium radius and the dot indicates the derivative with respect to time.

In the following, the matched asymptotic solution method will be employed in order to derive an equation for the radial dynamics of the bubble, which is based on matching the near field and the far field expressions for v and p. The assumption of incompressibility implies

$$v_r = -\frac{\dot{R}(t)R^2(t)}{r^2}. \tag{6}$$

Integration of (5) through the surrounding medium, from R to r in the near field gives:

$$p_{\text{in}} - p_{\text{L}} = -\rho_0 \left(R\ddot{R} + \frac{3}{2}\dot{R}^2 \right) + \frac{\rho_0}{r} f' - \frac{\rho_0}{2}\frac{f^2}{r^4} + \tau_{rr}|_R^r + 3\int_R^r \frac{\tau_{rr}}{r} dr, \tag{7}$$

where $f = R^2\dot{R}$, p_{L} is the pressure outside the bubble wall, p_{in} is the pressure in the internal zone at a distance r and ' indicates the total derivative. Note that the expression $-\rho_0 f'/r$ equals the radiated pressure by a pulsating bubble at a distance r.

In the far field stress components and the nonlinear convection terms are negligible; the linear acoustic equation can be obtained upon eliminating p between (1) and (3) as (Prosperetti and Lezzi [1986]):

$$\nabla^2\varphi - \frac{1}{c^2}\frac{\partial^2\varphi}{\partial t^2} = 0, \tag{8}$$

where φ is the velocity potential, i.e. $\vec{v} = \nabla\varphi$. The solution to (8) has the form

$$\varphi_{\text{ex}} = \frac{1}{r}\left[\psi_1\left(t - \frac{r}{c}\right) + \psi_2\left(t + \frac{r}{c}\right)\right], \tag{9}$$

where ψ_1/r and ψ_2/r characterize an incident and outgoing spherical wave, respectively. The expression for the pressure in the far field follows as (Prosperetti and Lezzi [1986])

$$p_{\text{ex}} = p_0 - \rho_0\frac{\partial\varphi_{\text{ex}}}{\partial t}. \tag{10}$$

2.1 Matching asymptotic solutions

In order to match the near field and far field solutions in the intermediate zone, the volumetric flow and the pressure matching conditions should be applied:

$$4\pi r^2 v_{r(\text{in})}\big|_{r\to\infty} = 4\pi r^2 v_{r(\text{ex})}\big|_{r\to 0} \qquad p_{\text{in}}|_{r\to\infty} = p_{\text{ex}}|_{r\to 0}. \tag{11}$$

Assuming the stresses vanish as $r \to \infty$, neglecting second order convective terms, and matching the solutions for pressure in (7) and (10) yields:

$$\rho_0\left(R\ddot{R} + \frac{3}{2}\dot{R}^2\right) = p_{\text{L}} + \frac{\rho_0}{r}f'\Big|_{r\to\infty} - p_0 + \rho_0\frac{\partial\varphi_{\text{ex}}}{\partial t}\Big|_{r\to 0} - \tau_{rr}(R,t) + 3\int_R^\infty \frac{\tau_{rr}}{r}dr \tag{12}$$

The time retarded quantity $\rho_0 f(t - r/c)'/r$ in (12) can be expanded into Taylor series as

$$\frac{\rho_0}{r} f'\left(t-\frac{r}{c}\right) \cong \frac{\rho_0}{r} f'(t) - \frac{\rho_0}{c} f''(t) + O(c^{-2}) \tag{13}$$

in which the first term on the right hand side vanishes as $r \to \infty$. Further, the time derivative of the velocity potential possesses a division by zero as $r \to 0$. It can be evaluated as

$$\left.\frac{\partial \varphi_{\mathrm{ex}}}{\partial t}\right|_{r\to 0} = \frac{\partial}{\partial t} \left.\frac{d\left[\psi_1\left(t-\frac{r}{c}\right)+\psi_2\left(t+\frac{r}{c}\right)\right]/dr}{r'}\right|_{r\to 0} = \frac{d}{dt}\frac{2\psi_2{}'(t)}{c} = 2\psi_2{}''(t)\,/c. \tag{14}$$

Inserting (13) and (14) into (12) gives

$$R\ddot{R} + \frac{3}{2}\dot{R}^2 = \frac{p_{\mathrm{L}} - p_0}{\rho} + \frac{2\psi_2'' + f''}{c} - \frac{\tau_{rr}(R,t)}{\rho} + \frac{3}{\rho}\int_R^{\infty} \frac{\tau_{rr}}{r} dr \tag{15}$$

The above equation includes third order derivative of R because of the term f''/c and it can be eliminated by subtracting a term which is at the order of accuracy $O(c^{-1})$. Multiplying (15) with R/c, taking the time derivative and assuming f'''/c is small gives

$$\frac{R^2\dddot{R}}{c} + \frac{5R\dot{R}\ddot{R}}{c} + \frac{3}{2}\frac{\dot{R}^3}{c} \equiv \frac{f''}{c} - \frac{R\dot{R}\ddot{R}}{c} - \frac{1}{2}\frac{\dot{R}^3}{c} = \frac{d}{dt}\frac{R(p_{\mathrm{L}} - p_\infty)}{\rho c} \tag{16}$$

where p_∞ is the pressure at the infinity, $p_\infty = p_0 - 2\rho\psi_2''/c + \tau_{rr}(R,t) + 3\int_R^\infty \tau_{rr}/r dr$. Adding (15) and (16) results in the following equation for radial bubble dynamics which accounts for the compressibility of the surrounding medium to first order:

$$\left(1-\frac{\dot{R}}{c}\right)R\ddot{R} + \frac{3}{2}\left(1-\frac{\dot{R}}{3c}\right)\dot{R}^2 = \left(1+\frac{\dot{R}}{c}\right)\frac{p_{\mathrm{L}} - p_\infty}{\rho} + \frac{R}{\rho c}\frac{d}{dt}(p_{\mathrm{L}} - p_\infty) \tag{17}$$

where

$$p_{\mathrm{L}} - p_\infty = p_{\mathrm{g}} - \frac{2\sigma}{R} - p_0 + P_{\mathrm{A}} g(t) + 3\int_R^\infty \tau_{rr}/r dr. \tag{18}$$

In (18) $P_A g(t) = 2\rho\psi_2''/c$ is the time-dependent acoustic pulse with P_{A} being a positive real number that scales the driving pressure.

2.2 Evaluating stress components

The choice of Voigt model and thus the constitutive relation given in (19) is appropriate for most marine sediments such as saturated soils (Leighton [2007]) and for soft tissues in low megahertz frequency range (Yang and Church [2004] and references therein). However, relaxations to this form of the equation such as non-Newtonian behaviour of the host medium are discussed by several authors as mentioned in the Introduction which may be considered in the future stages of this research in order to model the rheological behaviour of clay- and mud-like sediments.

The constitutive relation of the Voigt model is given as (Church [1995])

$$\tau_{rr} = 2(G\,\gamma_{rr} + \mu\,\dot{\gamma}_{rr}) \tag{19}$$

where γ_{rr} is the strain, $\dot{\gamma}_{rr} = \partial v/\partial r$ is the strain rate, G is the shear modulus and μ is the viscosity of the medium. Using the incompressibility condition (6) in the near field, strain and strain rate can be evaluated as $\gamma_{rr} = -(2/3r^3)(R^3 - R_0^3)$ and $\dot{\gamma}_{rr} = -(2R^2/r^3)\dot{R}$, respectively. Upon evaluation of the integral term in (18), one obtains:

$$3\int_R^\infty \tau_{rr}/r dr = -\frac{4G}{3R^3}(R^3 - R_0^3) - \frac{4\mu\dot{R}}{R}. \tag{20}$$

2.3 Bubble dynamics

Using the results in the previous section obtained using Voigt constitutive relation, the Keller-Miksis type equation which describes the radial motion of a spherical bubble in an unbounded viscoelastic medium can be written as follows;

$$\rho\left(1 - \frac{\dot{R}}{c}\right)R\ddot{R} + \frac{3}{2}\rho\left(1 - \frac{\dot{R}}{3c}\right)\dot{R}^2 = \left(1 + \frac{\dot{R}}{c} + \frac{R}{c}\frac{d}{dt}\right)\left(p_{\mathrm{g}} - \frac{2\sigma}{R} - p_0 + P_{\mathrm{A}}g(t) - \frac{4\mu\dot{R}}{R} - \frac{4G}{3R^3}(R^3 - R_0^3)\right) \tag{21}$$

In order to complete the set of equations given above, the behaviour of the internal gas pressure of the bubble (p_{g}) should be known. In the undisturbed state (in the absence of acoustic excitation in the liquid), the following equation holds for the bubble's interior pressure;

$$p_{g_0} = p_0 + \frac{2\sigma}{R_0} \tag{22}$$

where p_{g_0} is the bubble interior pressure at equilibrium. The most common way of calculating p_g is to appeal to the polytrophic law

$$p_g = p_{g_0}\left(\frac{R_0}{R}\right)^{3\kappa} \tag{23}$$

where κ is the polytrophic exponent which take the value 1 for isothermal conditions and the value γ for adiabatic conditions. In the above model, the temperature within the bubble is assumed to be uniform. Unless the value of κ changes during the oscillatory cycle, which is rarely allowed to do in most studies, Eq. (23) can never predict any net thermal losses.

In order to account for the thermal processes more precisely, the continuity and the energy conservation equations for a perfect gas would need to be solved, which are given respectively by

$$\frac{D\rho_g}{Dt} + \rho_g \nabla \cdot \vec{v}_g = 0 \tag{24}$$

$$\rho_g C_p \frac{DT}{Dt} + \frac{T}{\rho}\frac{\partial \rho_g}{\partial t}\bigg|_p \frac{Dp_g}{Dt} = \nabla \cdot (K\nabla T). \tag{25}$$

In above equations, ρ_g is the density of the gas, $\vec{v}_g$ is the velocity field within the bubble, T is the temperature, C_p is the specific heat at constant pressure, and K is the thermal conductivity of the gas. This formulation still assumes the uniformity of the internal pressure. However, it provides the ability to model the temperature profile within the bubble, thus an estimate of the heat flux from the thermal boundary layer near the bubble wall. Unsurprisingly, this approach is computationally expensive since it requires the evaluation of the spatial distribution of the temperature field at each acoustic cycle by using numerical integration schemes (Kamath and Prosperetti [1989]).

The above formulation can be modelled to first order accuracy by using an artificial thermal viscosity term μ_{th} though the detailed derivation will not presented here and can be found in Prosperetti et al. [1988]. By doing so, the equation for the internal pressure (23) is modified as

$$p_g = p_{g_0}\left(\frac{R_0}{R}\right)^{3\kappa(\omega)} - 4\mu_{th}\frac{\dot{R}}{R} \tag{26}$$

where $\mu_{\mathrm{th}} = (p_{\mathrm{g_o}}/4\omega)Im(\Phi)$ is the "thermal viscosity", ω is the angular frequency, and

$$\Phi = \frac{3\gamma}{1 - 3(\gamma - 1)i\chi[\left(\frac{i}{\chi}\right)^{\frac{1}{2}} coth\left(\frac{i}{\chi}\right)^{\frac{1}{2}} - 1]}. \tag{27}$$

with γ being the polytrophic exponent during adiabatic behaviour of the gas content, $\chi = D/\omega R_0^2$ representing the thermal diffusion length and D is the thermal diffusivity of the gas. The *effective* polytrophic index in (27) obeys the relation

$$\kappa(\omega) = \frac{1}{3} Re(\Phi) \tag{28}$$

The derivative of the bubble interior pressure can be evaluated as

$$\dot{p_{\mathrm{g}}} = -3\kappa p_{\mathrm{g_o}} \left(\frac{R_0}{R}\right)^{3\kappa} \frac{\dot{R}}{R} - 4\mu_{\mathrm{th}} \left(-\frac{\dot{R}^2}{R^2} + \frac{\ddot{R}}{R}\right) \tag{29}$$

2.4 Analytical solutions

An analytical solution to equation (21) may be obtained by assuming small perturbations of the bubble radius; i.e. $R=R_0(1+x(t))$ where x <<1. In order to study the second order harmonics, the second order terms in x are retained;

$$\begin{aligned} &\dot{R} = R_0\dot{x}, && \ddot{R} = R_0\ddot{x}, \\ &R^{-1} = R_0^{-1}(1 - x + x^2), \\ &R^{-3\kappa} = R_0^{-3\kappa}(1 - 3\kappa x + \tfrac{3\kappa(3\kappa+1)}{2} x^2). \end{aligned} \tag{30}$$

Assuming polytrophic behaviour of the bubble interior, the spatially uniform bubble pressure (26) and its derivative (29), can be expanded by the use of (30) as

$$p_{\mathrm{g}} = p_{\mathrm{g_o}} \left(1 - 3\kappa x + \frac{3\kappa(3\kappa + 1)}{2} x^2\right) - 4\mu_{\mathrm{th}}\dot{x} + 4\mu_{\mathrm{th}}\dot{x}x \tag{31}$$

and

$$\dot{p_{\mathrm{g}}} = -3\kappa p_{\mathrm{g_o}}\dot{x} + 3\kappa(3\kappa + 1)p_{\mathrm{g_o}}\dot{x}x - 4\mu_{\mathrm{th}}(\ddot{x} - \dot{x}^2 - \ddot{x}x) \tag{32}$$

Substitution of equations (30-32) into (21), only retaining second order terms, using the definition of the equilibrium pressure for the bubble interior (23), and assuming that $g(t) \sim e^{i\omega t}$ yields;

$$\left(\rho R_0^2 + \frac{4(\mu_{\text{th}} + \mu)R_0}{c}\right)\ddot{x} + \rho R_0^2 \ddot{x}x + \frac{3}{2}\rho R_0^2 \dot{x}^2 + \left[\left(3\kappa p_{\text{g}_0} - \frac{2\sigma}{R_0} + 4G\right)\frac{R_0}{c} + (4\mu + 4\mu_{\text{th}}) - P_A g(t)\frac{R_0}{c}\right]\dot{x} - \left[\left(3\kappa(3\kappa - 1)p_{\text{g}_0} + 8G\right)\frac{R_0}{c} + 4(\mu_{\text{th}} + \mu)\right]\dot{x}x + \left[3\kappa p_{\text{g}_0} - \frac{2\sigma}{R_0} + 4G - P_A g(t)\frac{i\omega R_0}{c}\right]x - \left[\frac{3\kappa(3\kappa + 1)}{2}p_{g_0} - \frac{2\sigma}{R_0} + 8G\right]x^2 = P_A g(t)\left(1 + \frac{i\omega R_0}{c}\right) \tag{33}$$

The term $P_A g(t)(i\omega R_0/c)$ in brackets multiplying x is to first order equivalent to the linear expression for the radiated pressure wave (Landau and Lifshitz [1958])

$$P_{sac} = \frac{\rho \ddot{R} R_0}{\left(1 - \frac{i\omega R_0}{c}\right)} \tag{34}$$

and therefore can be further written as

$$P_A g(t)\frac{i\omega R_0}{c} \approx \frac{\rho \ddot{R} R_0}{\left(1 - \frac{i\omega R_0}{c}\right)} = \frac{-\omega^2 \rho R_0^2 x}{1 + (\omega R_0/c)^2}. \tag{35}$$

Furthermore the last term multiplying $\dot{x}$ in (33) can be arranged as;

$$P_A g(t)\frac{R_0}{c} \approx \frac{1}{i\omega}P_{sac} = \frac{1}{i\omega}\frac{\rho R_0^2(-\omega^2 x)}{1 + (\omega R_0/c)^2}\left(1 + \frac{i\omega R_0}{c}\right) = \frac{\rho R_0^2(-\omega^2 x)}{1 + (\omega R_0/c)^2}\left(\frac{R_0}{c} + \frac{1}{i\omega}\right), \tag{36}$$

the real part of which gives

$$P_A g(t)\frac{R_0}{c} \approx \frac{-(\omega R_0/c)}{1 + (\omega R_0/c)^2}\omega(\rho R_0^2). \tag{37}$$

Inserting (37) and (35) into (33), one obtains

$$\left(\rho R_0^2 + \frac{4(\mu_{\text{th}} + \mu)R_0}{c}\right)\ddot{x} + \rho R_0^2 \ddot{x} x + \frac{3}{2}\rho R_0^2 \dot{x}^2 \tag{38}$$
$$+ \left[\left(3\kappa p_{\text{g}_0} - \frac{2\sigma}{R_0} + 4G\right)\frac{R_0}{c} + (4\mu + 4\mu_{\text{th}}) + \frac{(\omega R_0/c)}{1 + (\omega R_0/c)^2}\omega(\rho R_0^2)\right]\dot{x}$$
$$- \left[\left(3\kappa(3\kappa - 1)p_{\text{g}_0} + 8G\right)\frac{R_0}{c} + 4(\mu_{\text{th}} + \mu)\right]\dot{x}x$$
$$+ \left[3\kappa p_{\text{g}_0} - \frac{2\sigma}{R_0} + 4G + \frac{\omega^2 \rho R_0^2}{1 + (\omega R_0/c)^2}\right]x$$
$$- \left[\frac{3\kappa(3\kappa + 1)}{2}p_{\text{g}_0} - \frac{2\sigma}{R_0} + 8G\right]x^2 = P_A g(t)\left(1 + \frac{i\omega R_0}{c}\right)$$

The linear part of (38) has the form,

$$m\ddot{x} + b\dot{x} + kx = -P_A e^{i\omega t} \tag{39}$$

where the effective mass, m, total damping, b_{tot}, and stiffness, k, are given by

$$m = \rho R_0^2 + \frac{4(\mu_{\text{th}} + \mu)R_0}{c}, \tag{40a}$$

$$b_{\text{tot}} = \left(3\kappa p_{\text{g}_0} - \frac{2\sigma}{R_0} + 4G\right)\frac{R_0}{c} + (4\mu + 4\mu_{\text{th}}) + \frac{(\omega R_0/c)}{1 + (\omega R_0/c)^2}\omega(\rho R_0^2), \tag{40b}$$

$$k = 3\kappa p_{\text{g}_0} - \frac{2\sigma}{R_0} + 4G + \frac{\omega^2 \rho R_0^2}{1 + (\omega R_0/c)^2} \tag{40c}$$

Note that equations (40) are the same as those found in Yang and Church [2004] except that the effective mass and thermal damping are increased by an amount proportional to μ_{th} which arises because of the use of artificial thermal damping. Comparison of (39) with that of a damped harmonic oscillator,

$$\ddot{x} + 2\beta_{\text{tot}}\dot{x} + \omega_0^2 x = -\frac{P_A e^{i\omega t}}{m} \tag{41}$$

where β_{tot} is the total damping and ω_0 is the natural frequency, yields expressions for the five components of damping (viscous, thermal, acoustic, interfacial and elastic) as,

$$\beta_{\text{vis}} = \frac{b_{\text{vis}}}{2m} = 2\mu / \left(\rho R_0^2 + \frac{4(\mu_{\text{th}} + \mu)R_0}{c}\right), \tag{42a}$$

$$\beta_{\mathrm{th}} = \frac{b_{\mathrm{th}}}{2m} = \left(\frac{3\kappa p_{\mathrm{g_o}} R_0}{2c} + 2\mu_{\mathrm{th}}\right) / \left(\rho R_0^2 + \frac{4(\mu_{\mathrm{th}} + \mu) R_0}{c}\right), \tag{42b}$$

$$\beta_{\mathrm{ac}} = \frac{b_{\mathrm{ac}}}{2m} = \frac{(\omega R_0/c)}{1 + (\omega R_0/c)^2} \frac{\omega}{2} (\rho R_0^2) / \left(\rho R_0^2 + \frac{4(\mu_{\mathrm{th}} + \mu) R_0}{c}\right), \tag{42c}$$

$$\beta_{\mathrm{int}} = \frac{b_{\mathrm{int}}}{2m} = -\sigma / (\rho c R_0^2 + 4(\mu_{\mathrm{th}} + \mu) R_0)\ , \tag{42d}$$

$$\beta_{\mathrm{el}} = \frac{b_{\mathrm{el}}}{2m} = 2G / (\rho c R_0 + 4(\mu_{\mathrm{th}} + \mu))\ , \tag{42e}$$

where

$$\beta_{\mathrm{tot}} = \beta_{\mathrm{vis}} + \beta_{\mathrm{th}} + \beta_{\mathrm{ac}} + \beta_{\mathrm{int}} + \beta_{\mathrm{el}}, \tag{42f}$$

and the natural frequency satisfies

$$\omega_0^2 = \left[3\kappa p_{\mathrm{g_o}} - \frac{2\sigma}{R_0} + 4G + \frac{\omega^2 \rho R_0^2}{1 + (\omega R_0/c)^2}\right] \Bigg/ \left(\rho R_0^2 + \frac{4(\mu_{\mathrm{th}} + \mu) R_0}{c}\right). \tag{43}$$

2.5 Harmonic expansions

In this section, the second order terms in equation (38) are maintained together with the linear elements of the equation since the second order components of the acoustic propagation are also of interest. Note that Yang and Church analysed only the first harmonic component. Church [1995] presented the second harmonic components for an encapsulated bubble in an incompressible viscoelastic medium. Here, the same notation will be used though the modified expression will be evaluated for a bubble without a shell, in a compressible viscoelastic medium. Equation (38) may be rearranged in the form,

$$\ddot{x} + \alpha_{\mathrm{n}} \ddot{x} x + \alpha_{\mathrm{dn}} \dot{x}^2 + \delta_{\mathrm{d}} \dot{x} - \delta_{\mathrm{dn}}\, \dot{x} x + \omega_0^2 x - \omega_{0\mathrm{n}}^2 x^2 = -\frac{P_A \sin \omega t}{m} \tag{44}$$

where

$$\alpha_{\mathrm{n}} = \rho R_0^2 / m \tag{45a}$$

$$\alpha_{\mathrm{dn}} = \frac{3}{2} \alpha_{\mathrm{n}} \tag{45b}$$

$$\delta_{\mathrm{d}} = 2\beta_{\mathrm{tot}} \tag{45c}$$

$$\delta_{\mathrm{dn}} = \left[\left(3\kappa(3\kappa-1)p_{\mathrm{g_o}} + 8G\right)\frac{R_0}{c} + 4(\mu_{\mathrm{th}} + \mu)\right]\Big/_{m} \tag{45d}$$

$$\omega_{\mathrm{0n}}^2 = \left[\frac{3\kappa(3\kappa+1)}{2}p_{\mathrm{g_o}} - \frac{2\sigma}{R_0} + 8G\right]\Big/_{m} \tag{45e}$$

Equation (44) is nonlinear (second order), thus a potential solution has the form (Church [1995])

$$x(t) = X_0 + X_1 \sin(\omega t + \phi_1) + X_2 \cos(2\omega t + \phi_2) \tag{46}$$

where X_0 is the change in the time-average radius due to nonlinear response of the bubble, X_1 is the amplitude of the first harmonic pulsation and X_2 is the second harmonic pulsation. The former and the latter are assumed to be relatively small compared to X_1, i.e. $1 > X_1 > X_0 \sim X_2$, therefore only terms of order X_1, X_1^2, X_0, and X_2 are retained in the expansions. The values and phases determined in this way are

$$X_0 = \frac{X_1^2}{2\omega_0^2}\left[-\frac{1}{2}\,\alpha_{\mathrm{n}}\omega^2 + \omega_{\mathrm{0n}}^2\right], \tag{47a}$$

$$X_1 = P_{\mathrm{A}}\chi_1/m, \tag{47b}$$

$$X_2 = \frac{X_1^2}{2}Y\chi_2, \tag{47c}$$

$$\phi_1 = \arctan[\omega\delta_{\mathrm{d}}/(\omega^2 - \omega_0^2)], \tag{47d}$$

and

$$\phi_2 = \arctan\left[\frac{B_{\mathrm{r}}\sin 2\phi_1 - B_{\mathrm{i}}\cos 2\phi_1}{B_{\mathrm{r}}\cos 2\phi_1 + B_{\mathrm{i}}\sin 2\phi_1}\right], \tag{47e}$$

where

$$\chi_1 = [(\omega^2 - \omega_0^2)^2 + (\omega\delta_{\mathrm{d}})^2]^{-1/2}, \tag{48a}$$

$$\chi_2 = \left[4\omega^2\delta_{\mathrm{d}}^2 + (\omega_0^2 - 4\omega^2)^2\right]^{-1/2}, \tag{48b}$$

$$Y = \left[\omega^2\delta_{\mathrm{d}}^2 + \left(\frac{5}{2}\alpha_{\mathrm{n}}\omega^2 + \omega_{0\mathrm{n}}^2\right)^2\right]^{1/2}, \tag{48c}$$

$$B_{\mathrm{r}} = -(\omega_0^2 - 4\omega^2)\left[\frac{5}{2}\alpha_n\omega^2 + \omega_{0\mathrm{n}}^2\right] - 2\omega^2\delta_{\mathrm{d}}\delta_{\mathrm{dn}}, \tag{48d}$$

and

$$B_{\mathrm{i}} = (\omega_0^2 - 4\omega^2)\omega\delta_{\mathrm{dn}} - 2\omega\delta_{\mathrm{d}}\left[\frac{5}{2}\alpha_{\mathrm{n}}\omega^2 + \omega_{0\mathrm{n}}^2\right]. \tag{48e}$$

2.6 Scattering Cross Sections

Scattering cross section of a bubble may be defined as the ratio of the total acoustic power scattered by an object at a particular frequency to the incoming acoustic intensity I_0:

$$\sigma_{\mathrm{s}} = \frac{4\pi r^2 I_{\mathrm{s}}}{I_0} \tag{49}$$

where $I_0 = |P_{\mathrm{A}}|^2/2\rho c$ and $I_{\mathrm{S}} = |P_{\mathrm{S}}|^2/2\rho c$. The amplitude of a scattered pressure wave, for a spherical bubble oscillating at low amplitude, is given by

$$P_{\mathrm{S}} = \frac{i\omega\rho R_0^2 U}{r} e^{-ikr} \tag{50}$$

with $k = \omega/c$ (the acoustic wave number) and $U = R_0\dot{x}$.

Using (48b) to define X_1, the scattering cross section at the first harmonic can be evaluated as

$$\sigma_{\mathrm{s}} = \frac{4\pi R_0^2\omega^4\rho^2 R_0^4\chi_1^2}{m^2} \tag{51}$$

Neglecting the thermal and viscous contributions to the effective mass, i.e. $m \approx \rho R_0^2$, and using the expression (48a) for χ_1 gives

$$\sigma_{\mathrm{s}} = \frac{4\pi R_0^2\omega^4}{(\omega^2 - \omega_0^2)^2 + \omega^2\delta_{\mathrm{d}}^2} = \frac{4\pi R_0^2\omega^4}{(\omega^2 - \omega_0^2)^2 + 4\beta_{\mathrm{tot}}^2\omega^2} \tag{52}$$

The above equation was used by Yang and Church [2004] (their Eq. (25)) with a typographical error which omits the factor 4 multiplying the term $\beta_{\mathrm{tot}}^2\omega^2$. It is noted here that their results (their Fig. 4) inherited this typographical error. Nevertheless, Ainslie and Leighton [2011] noted that the above expression for the scattering cross-section involves an error because of a missing *second order* term in ε (where $\varepsilon \equiv \omega R_0/c$) in the expansion of $\exp(-ikr)$ in (50) and gave the corrected expression as

$$\sigma_s = \frac{4\pi R_0^2}{\left(\frac{\omega_0^2}{\omega^2} - 1 - 2\frac{\beta_0}{\omega}\varepsilon\right)^2 + \left(2\frac{\beta_0}{\omega} + \frac{\omega_0^2}{\omega^2}\varepsilon\right)^2} \tag{53}$$

where β_0 is the total of the damping coefficients other than acoustic damping.

3 Results

3.1 Examples for soft tissue (Yang and Church 2005)

3.1.1 Resonance frequency

In this section, Fig. 1 of Yang and Church is re-plotted. The expression for the resonance frequency is given by (43) and it is highly dependent on the viscoelastic properties of the medium, i.e. the shear modulus. In Fig. 1, it can be seen that the resonance frequency decreases with increasing bubble radius. Further, for a given bubble radius, the resonance frequency increases with increasing shear modulus (*G*).

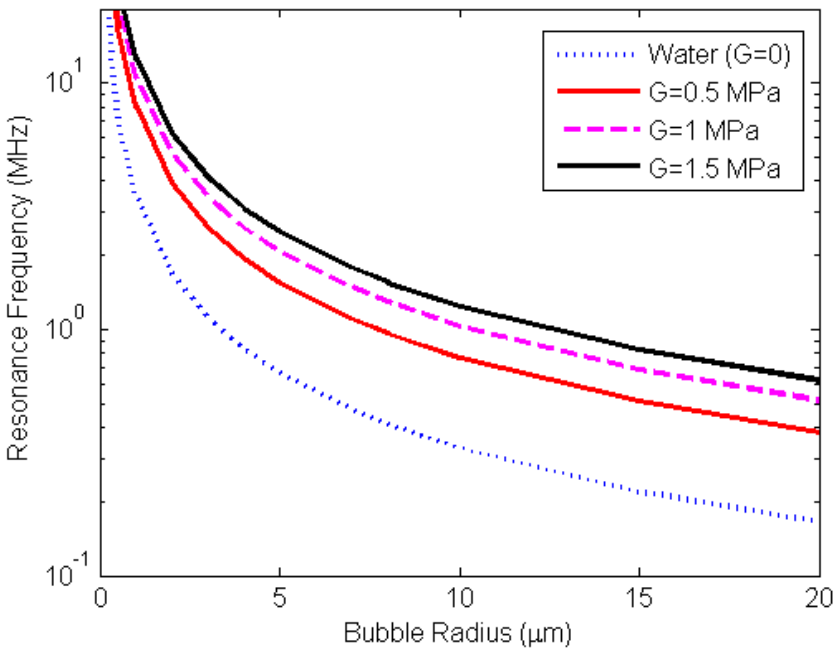

Figure 3.1: Resonance frequency of air bubbles in water and in viscoelastic mediums with different shear moduli.

3.1.2 Linear damping coefficients

In this section, the computed damping coefficients are plotted versus driving frequency for a fixed bubble radius and versus bubble radius for a fixed driving frequency in Figs. 3.2 and 3.3, respectively. The thermal damping calculated using *thermal viscosity* in (26) (denoted as *"P-Th"*) differ from those in Yang and Church [2004] because their results are based on the formulation given by Prosperetti [1977]. Further, computed values using the polytrophic relation (23) are also plotted as was done by Yang and Church. It should be noted that nonlinear, time-dependent computations for the pressure and the temperature inside the bubble will be performed in Section 4 of this report by solving (24) and (25), thus a quantification of the inaccuracy involved in thermal and other loss mechanisms using linear models will be presented.

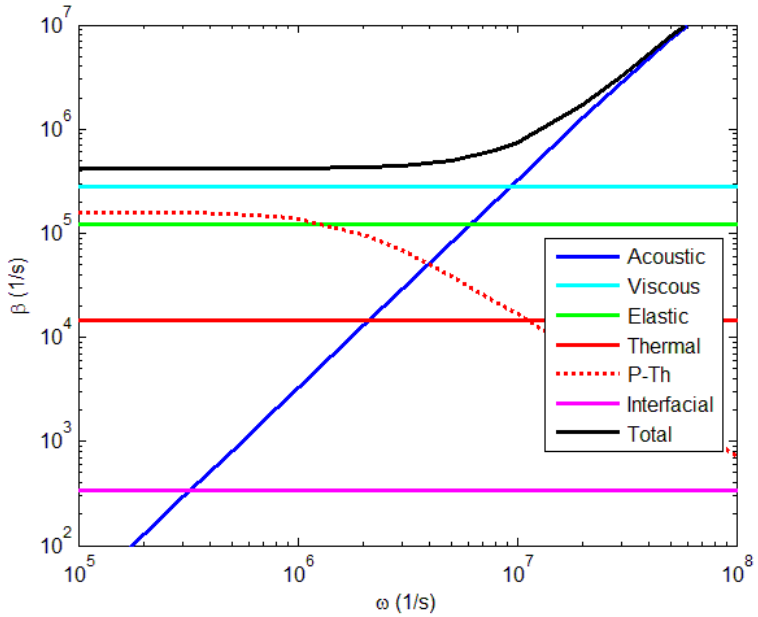

(a)

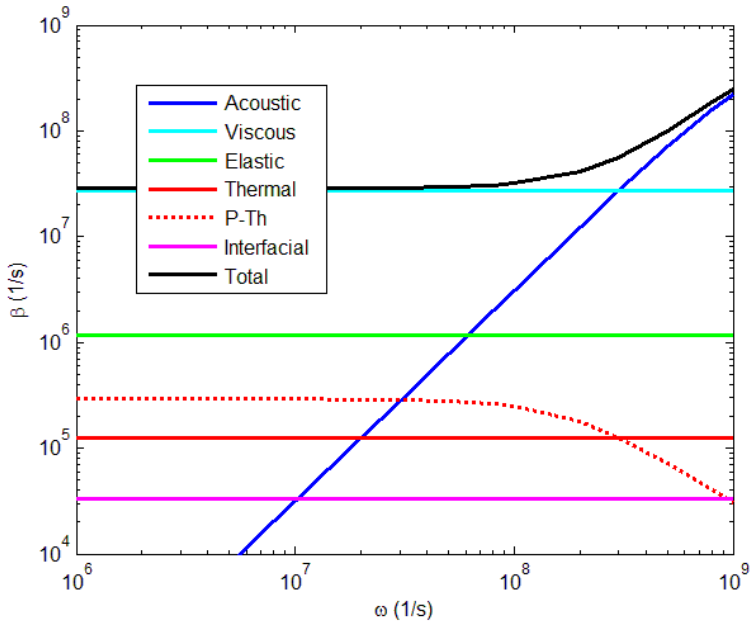

(b)

Figure 3.2: Damping coefficients versus radial driving frequency for a bubble with radius (a) 10 µm and (b) 1µm, surrounded by a medium with G=1 MPa and µ=0.015 Pa s.

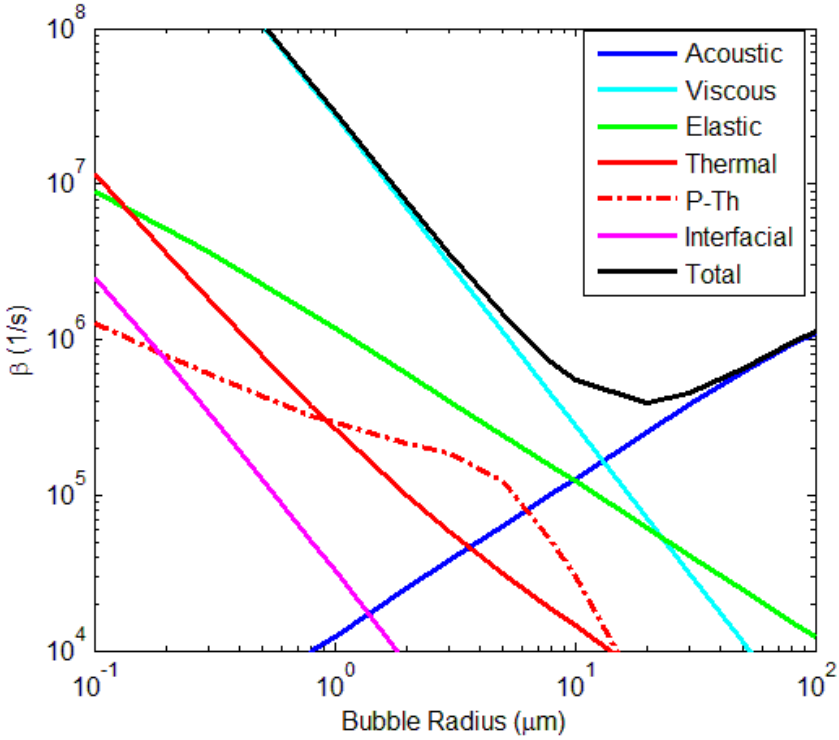

(a)

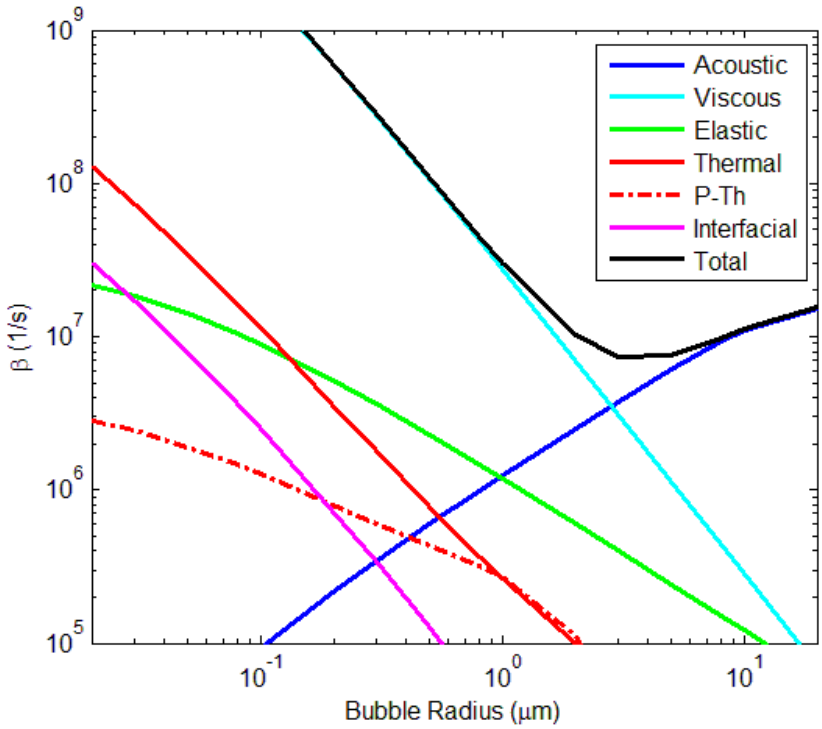

(b)

Figure 3.3: Damping coefficients versus equilibrium radius for radial frequencies of (a) 1 MHz and (b) 10 MHz, for air bubbles in a medium with G=1 MPa and μ=0.015 Pa s.

3.1.3 Scattering cross sections

The results for scattering cross-sections as obtained by Yang and Church are re-plotted here by using the formula which contains a typographical error (their Eq. 25), thus demonstrating the effect of the error. In Figure 3.4, the scattering cross-section over a range of bubble radii is plotted using driving frequencies of 1 MHz and 10 MHz. The effect of tissue elasticity in these results is to shift the resonance peak to larger bubble radii when compared to the resonance peak in water. Additionally, the cross-sections for bubbles in tissue are less (in some cases by one order of magnitude), indicating that bubbles in a viscoelastic medium are more difficult to detect acoustically than bubbles in water at the same frequency. It should be noted that if the multiplication-by-4 error in the denominator of Yang and Church's equation was corrected, the cross-section values shown in Fig. 3.4 would be reduced.

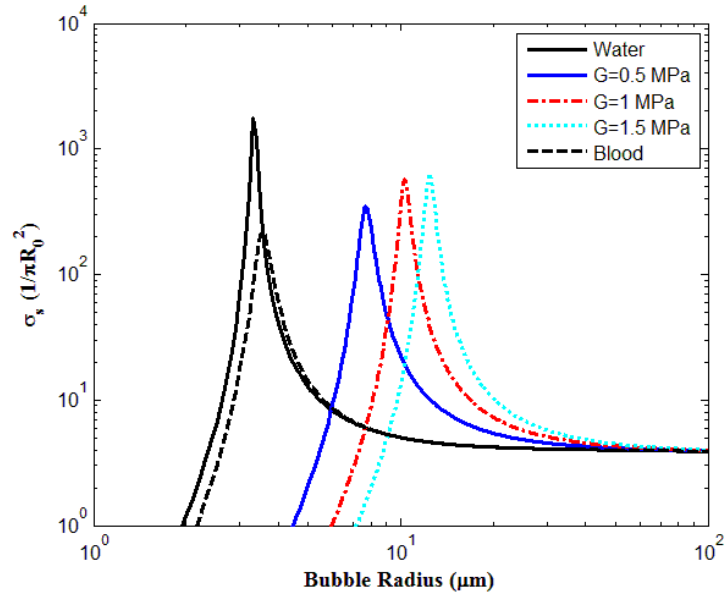

(a)

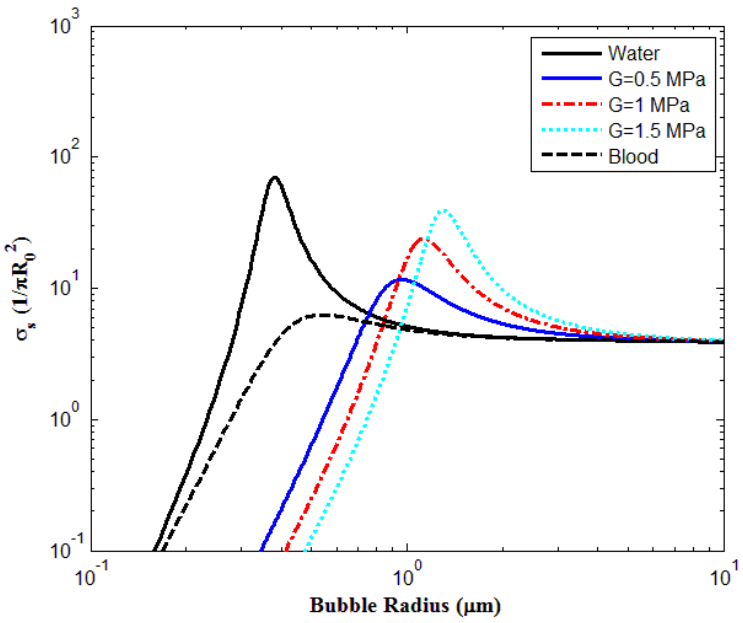

(b)

Figure 3.4: Scattering cross-sections versus bubble radius for driving frequencies of (a) 1 MHz and (b) 10 MHz.

Nevertheless, the above results reflect not only the typographical error involved in the formula of the scattering cross-section but also the largely unnoticed mistake in the derivation of an expression for the scattering cross-section. The corrected formula (53) was given by Ainslie and Leighton [2011] and the above results are replotted in Fig. 3.5, based on their formulation. It can be noted that the values of the cross-sections are less than the values reported by Yang and Church for all of the cases. Further, careful inspection of the graphs

reveals the shifts to the resonance peaks which are due to a fractional correction to the resonance frequency in the new formulation (amounting to $\beta_0(\omega_0)R_0/c$) as noted by Ainslie and Leighton [2009]).

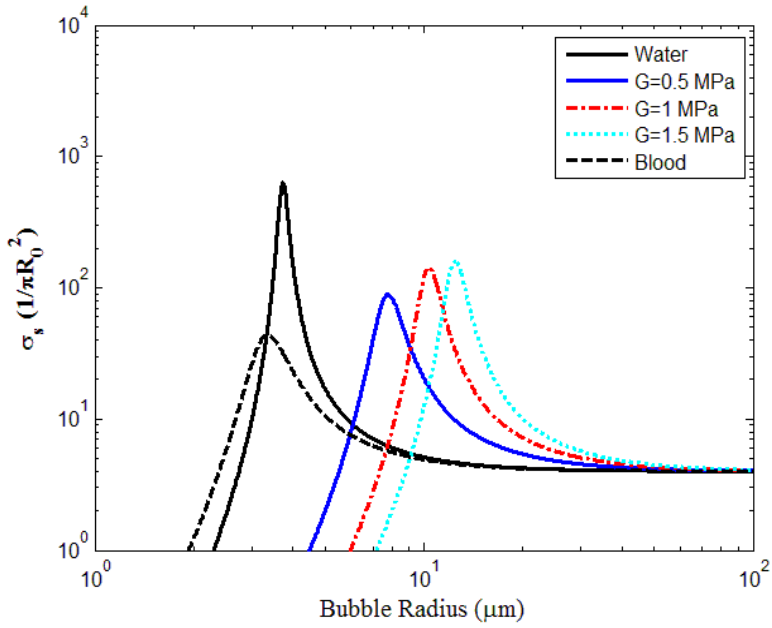

(a)

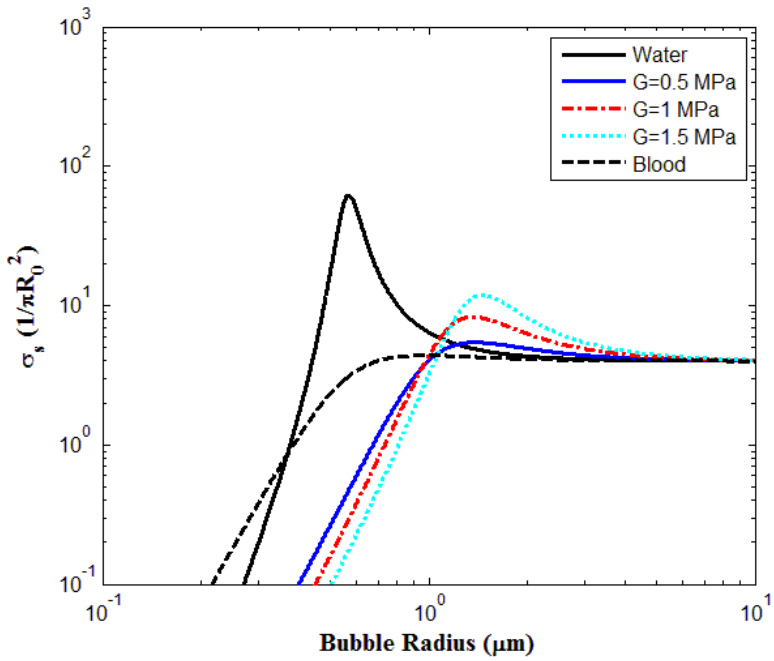

(b)

Figure 3.5: Scattering cross-sections versus bubble radius for driving frequencies of (a) 1 MHz and (b) 10 MHz using the formulation of Ainslie and Leighton [2011].

3.1.4 Radius-time curves (Numerical Results)

The theory presented by Yang and Church aimed to provide an understanding of the behaviour of the cavitation bubbles in soft tissues which are usually driven by high amplitude ultrasonic fields. Under transient or stable cavitation conditions, bubble radius may increase even up to an order (or two) of magnitude larger of its initial value. In these conditions, linear models do not simulate the behaviour of the bubble radius accurately. Note that a further simplification used by Yang and Church was assuming the adiabatic behaviour of the gas inside the bubble, which suggests no heat transfer between the bubble content and the surrounding viscoelastic medium, which may be well violated in the case of stable cavitation since the bubble interior temperature may rise to a few thousand Kelvin (*Storey and Szeri* [2000]). At the instant of minimum bubble radius during the stable cavitation, bubble temperature reaches its highest and a thermal boundary layer forms inside the bubble, near the bubble wall, creating a heat flow from the bubble to the surrounding due to the high temperature gradient. Such heat transfer effects can be modelled more accurately by solving the set of equations (24)-(25) or alternatively by incorporating an ordinary differential equation derived from the first law of thermodynamics applied to the bubble content (Storey and Szeri [2000], Stricker et al. [2011]). In this report, the radius-time plots for bubbles in a viscoelastic medium are obtained by solving the Keller-Miksis type equation (1) together with equations (24)-(25) for the bubble interior pressure and temperature, respectively. In Figure 3.6, the radial response of a 1 μm air bubble driven by a 3.5 MHz pulse is plotted for in *vivo* and in *vitro* cases. This figure reproduces Fig. 6 of Yang and Church [2004]. The results obtained are almost identical, even though a quantification of the thermal losses due to the use of two different models (the nonlinear formulation and the polytrophic model) would be of interest and is left to later stages of this work. Similarly, the radial response of a 5 μm air bubble driven by a 3.5 MHz pulse, in *vivo* and in *vitro*, is plotted in Fig. 3.7 (which reproduces Fig. 7 of Yang and Church [2004]).

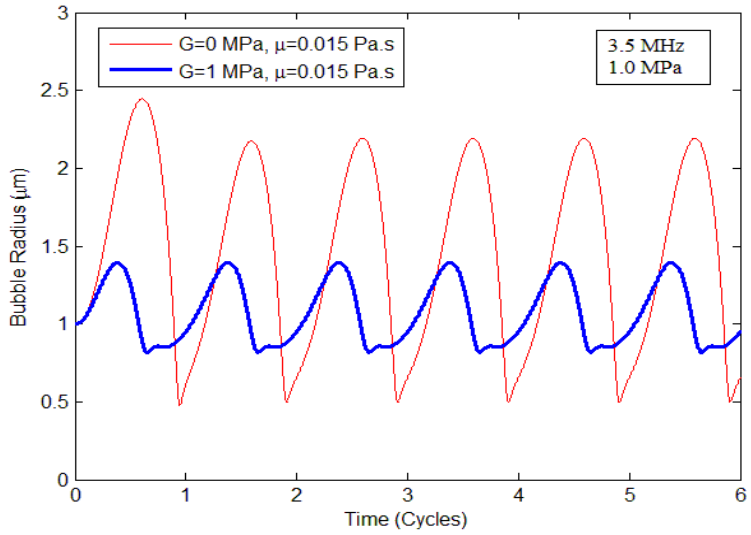

(a)

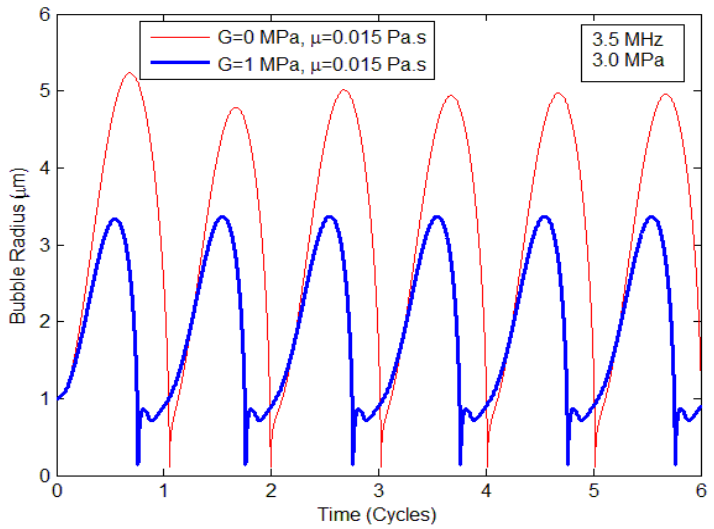

(b)

Figure 3.6: Radial responses of 1-μm bubbles driven by a 3.5 MHz pulse at (a) 1 MPa and (b) 3 MPa, for G=0 (thin line) and G=1 MPa (thick line).

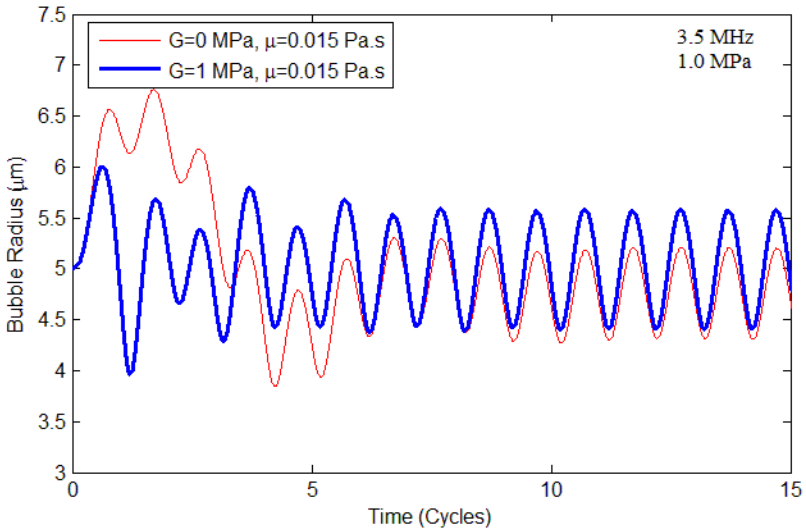

(a)

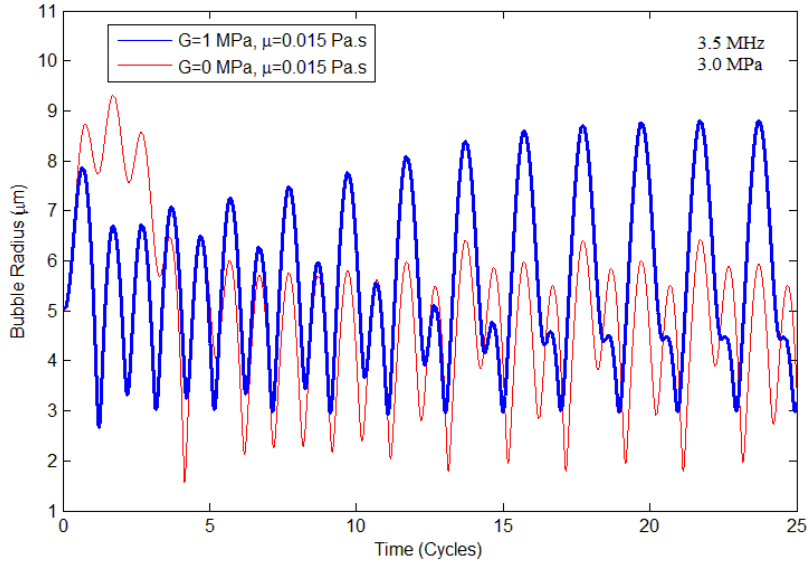

(b)

Figure 3.7: Radial responses of 5-μm bubbles driven by a 3.5 MHz pulse at (a) 1 MPa and (b) 3 MPa, for G=0 (thin line) and G=1 MPa (thick line).

3.1.5 Second harmonic emissions

The analytical solutions including the emissions up to second order harmonics as derived in Section 2.5 can provide the solution of the radial oscillations of bubbles at low pressure amplitudes without the need for a time dependent computation. In Figure 3.8, the dynamic pulsations of a 1 mm air bubble in a viscoelastic medium with material properties G=1 MPa, ρ = 1060 kg/m^3, μ = 0.015 Pa s and σ = 0.056 N/m are shown using both the time-dependent results obtained with MATLAB *ode45* and the analytical expressions given in Eqs. (44)-(48).

The acoustic pulse is chosen as a uniform sinusoid waveform with pressure amplitude P_A = 50 kPa and the wave frequency is set as 10 kHz.

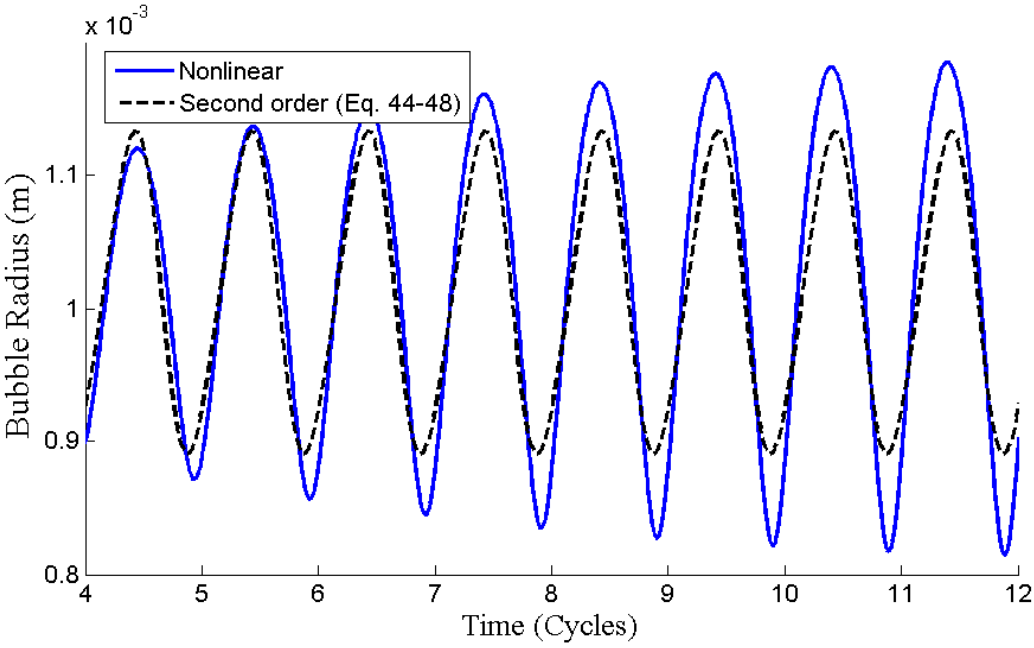

Figure 3.8: Radial response of a 1 mm bubble in a viscoelastic medium simulated by non-linear formulation (solid line) and the second order analytical solution (dashed line). Acoustic forcing is applied as a 10 kHz pulse with 50 kPa zero-to-peak amplitude.

3.2 Application of the model to sediments

The proposed model can be applied to sediments with several advantages over A&H model such as having no sign ambiguities in the speed of sound formula, defining the higher order scattering coefficients etc. In this section, the results obtained by applying the model to the marine sediments are presented and compared to those obtained by A&H model. As mentioned above the formulation of the A&H model is not explicitly stated in this report. Two different sediments types, ocean bottom silt and harbour mud, which were investigated in A&H papers (see Figs. 15 and 16 of Part II of their paper) will be examined here as well, to facilitate a direct comparison of two models. The mixture properties of ocean silt and harbour mud, as given in A&H, are listed in Table 1. Among the parameters, *porosity* refers to the void fraction of liquid in the sediment when there is no gas bubbles present. In the computations, where necessary (for example in the speed of sound and attenuation plots), the value of bubble gas volume fraction (β_G) is evaluated by multiplying porosity of each sediment sample by 0.1 (which is the value of n_g' in A&H).

Table 3.1: Model input parameters for harbour mud and ocean silt

	Harbour Mud	Ocean Silt
Porosity	0.75	0.68
Shear Modulus (G)	1 GPa	250 GPa
Bubble void fraction (β_G)	0.075	0.068
Density (ρ)	1400 kg/m^3	1550 kg/m^3
Speed of sound (c)	1488 m/s	1552 m/s

3.2.1 Linear damping coefficients

One major difference between the A&H theory and the current formulation is the use of non-dimensional damping coefficients in A&H. The non-dimensional damping coefficients for thermal and acoustic losses are used in their work following the theory of Spitzer [1948] which was originally written for bubbly liquids. The viscous damping is neglected in their work assuming that the frictional losses will occur due to the dynamic shear modulus only. They introduced a *complex* dynamic shear modulus $G^*=G+iG'$ where the imaginary part (G') of the shear modulus is a posteriori taken as one-fifth of the real part of G^* and used in the expression for viscoelastic losses (their Eq. (9) of Part II). In this section, the thermal, acoustic, elastic and viscous damping constants of the current formulation are plotted for air bubbles in ocean sediments and compared to the predictions from the A&H theory by assuming $\delta \equiv 2\beta/\omega$, where δ is the non-dimensional and β is the dimensional damping coefficient. Ainslie and Leighton [2009] noted that there exist three different definitions for δ, thus there is no simple explanation to define their relationship. More specifically, Spitzer's theory is identical to the Wildt-Medwin model (defined in Ainslie and Leighton [2009]) and has an incorrect expression for the frequency dependence of the radiation damping which persists in the expression for the scattering cross-section. Noticing the latter fact, A&H attempted to correct the expression for the scattering cross-section; though they did not present a rigorous analysis but an inconsistent formulation (see Ainslie and Leighton [2009] for details).

In Fig. 3.9, the linear damping coefficients for acoustic propagation in harbour mud are plotted as a function frequency for both formulations. It can be observed that the thermal losses (evaluated by using a thermal viscosity term) are higher than other losses when the frequency of the driving pulse is less than 1 kHz. In contrast, the radiation damping becomes dominant for frequencies higher than 10 kHz. Within the 1-10 kHz range, elastic damping

losses are the highest. According to A&H theory, the elastic damping is the largest source of losses for driving frequencies of less than 10 kHz. One may note that the elastic damping coefficient decreases with increasing frequency in A&H theory, whereas it remains constant in the current formulation.

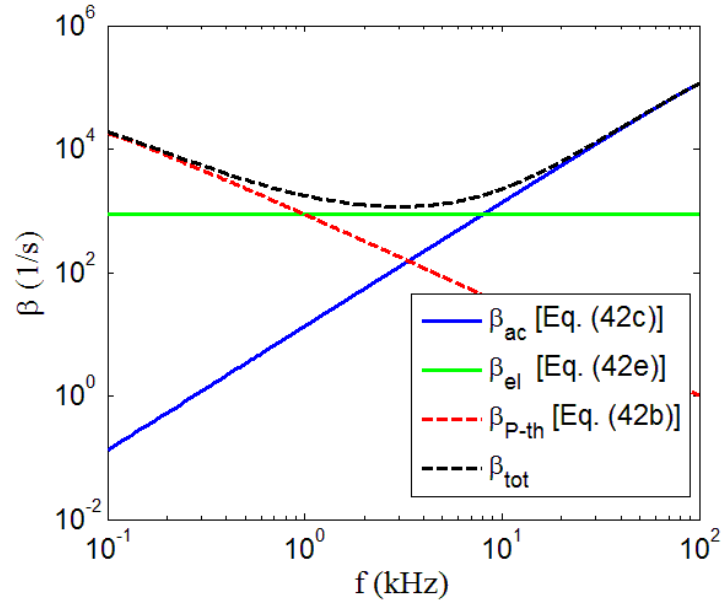

(a)

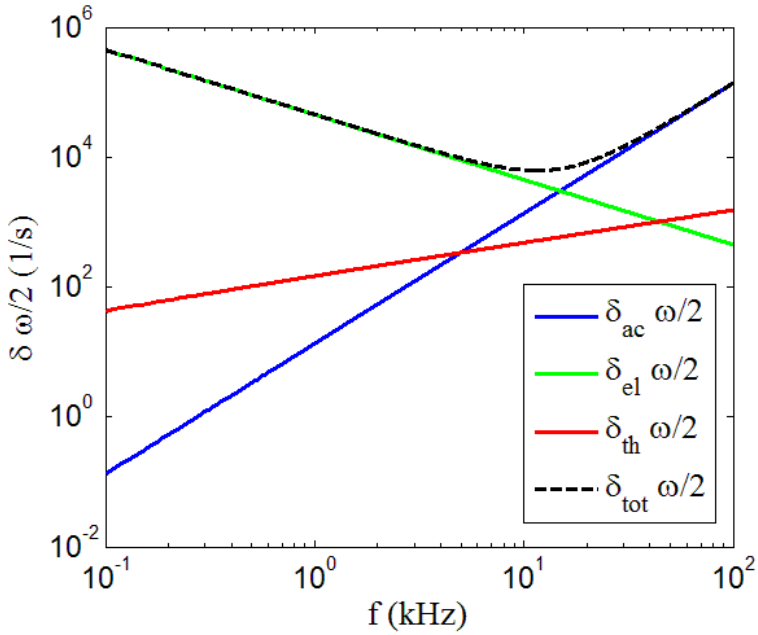

(b)

Figure 3.9: Damping coefficients vs driving frequency for a 1 mm equilibrium radius bubble in mud, by using (a) Eq. 42 and (b) the A&H theory with dimensional coefficients (δ ω/2).

In Fig. 3.10, the linear damping coefficients for acoustic propagation in ocean silt are plotted as a function frequency. It can be observed that the thermal losses (evaluated by using a thermal viscosity term) become important when the frequency of the driving pulse is very

low, i.e. less than 0.1 kHz. The radiation damping increases with driving frequency similar to the previous case. Nevertheless, the elastic damping is the largest loss mechanism in ocean silt for driving frequencies less than 10 kHz. Similarly, A&H theory predicts the friction losses to be the most dominant for these conditions; however it suggests that these losses decrease with increasing frequency.

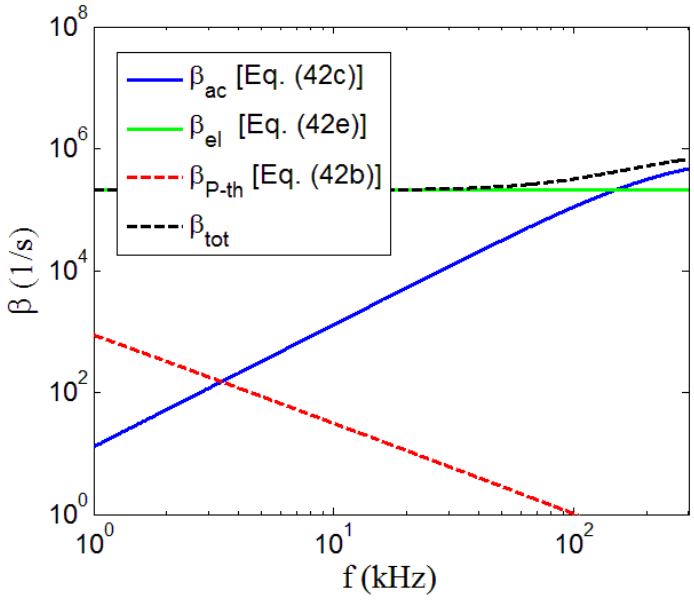

(a)

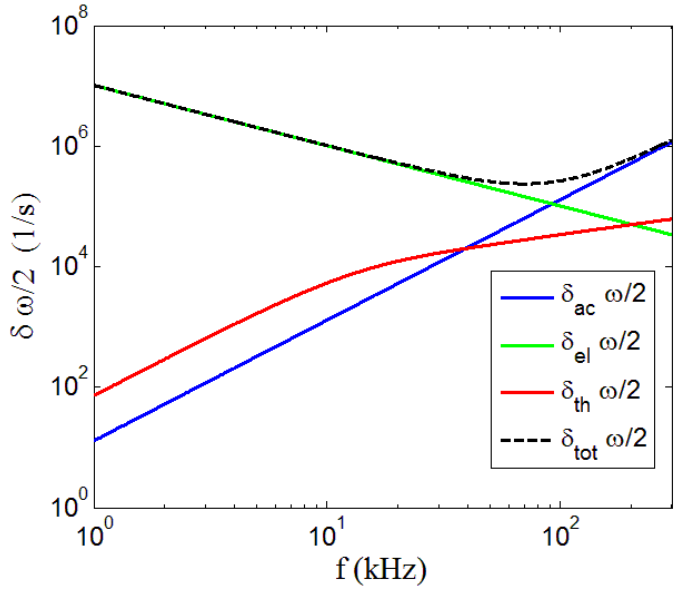

(b)

Figure 3.10: Damping coefficients vs driving frequency for a 1 mm equilibrium radius bubble in ocean silt, by using (a) the current formulation and (b) the A&H theory with dimensional coefficients (δ ω/2).

It is also useful to observe the behaviour of the damping coefficients with varying radius at a given driving frequency. In Fig. 3.11, the linear damping coefficients using the

current formulation are plotted for air bubbles in harbour mud at a pulse frequency of 10 kHz. The elastic damping, decreasing with increasing bubble radius, appears to be the most important loss mechanism. It is worthwhile to note that the thermal damping evaluated with the use of thermal viscosity gets higher than other damping constants for intermediate range size bubbles (10-100 μm), revealing the importance of the thermal model chosen for the bubble interior gas pressure. Also note that the radiation damping increases with equilibrium bubble radius and viscous damping becomes high only for very small equilibrium radii, i.e. ~1 μm. The results from the A&H theory are not plotted versus the bubble radius since at given conditions, both for harbour mud and ocean silt, the elastic damping dominates over, being at least a few orders of magnitude of higher than, the other loss mechanisms.

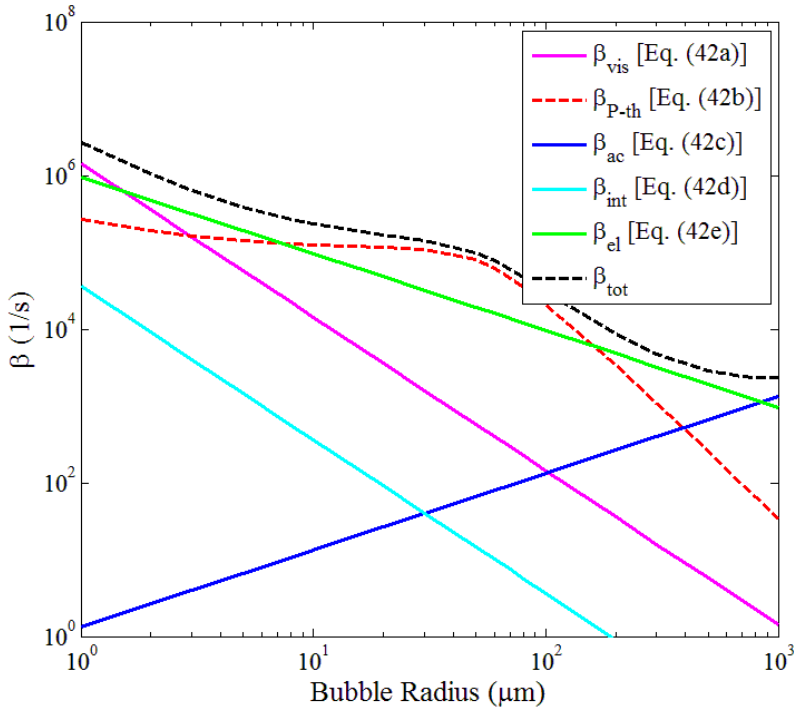

Figure 3.11: Damping coefficients vs equilibrium bubble radius in harbour mud at a pulse frequency of 10 kHz by using the current formulation.

In Fig. 3.12, the linear damping coefficients are plotted for air bubbles in ocean silt at a pulse frequency of 10 kHz. The elastic damping, similarly to the previous case, is the largest source of the dissipation. Among the other damping mechanisms, the thermal damping gets higher for intermediate range size bubbles (10-100 μm). Also note that the radiation damping increases with equilibrium bubble radius and viscous damping becomes high only for very small equilibrium radii, i.e. ~1 μm. The results from the A&H theory are

not plotted versus the bubble radius since at given conditions, both for harbour mud and ocean silt, the elastic damping dominates over, being at least a few orders of magnitude of higher than, the other loss mechanisms.

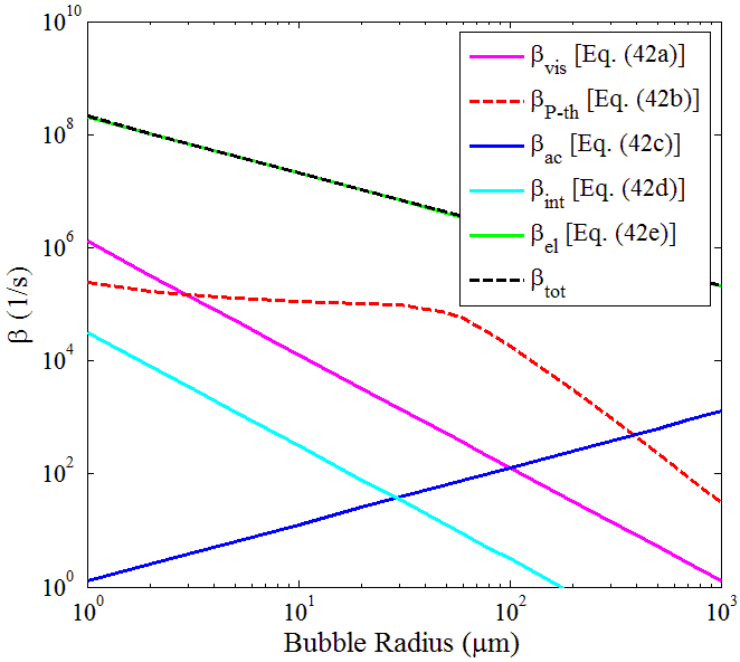

Figure 3.12: Damping coefficients vs equilibrium bubble radius in ocean silt at a pulse frequency of 10 kHz by using the current formulation.

3.2.2 Scattering cross section

Scattering cross-section (and/or the extinction cross-section) is one of the most commonly used measures in the estimation of bubble populations as it relates the energy of the incident wave to the scattered wave for each bubble radius. Owing to the wide range of assumptions with the physics of wave propagation in bubbly medium (more generally in water or in viscoelastic mediums as in this research), the formulations for the damping coefficients may differ significantly as shown in the previous sub-section which may, in turn, affect the value of the scattering cross-sections. In this section, the scattering cross-section, as predicted from two different theories, will be plotted. As previously mentioned, the original formulation of Yang and Church involves an error, therefore the recently derived formula of Ainslie and Leighton [2011] will be used in the computations. The theory of A&H involves an inconsistency: Their Eqn. (55) of Part I (abbreviation A&H-*n* will be used hereafter where *n* is the equation number) gives the correct dependency of radiation damping on the resonance and the driving frequencies; however, when the equation for the radiation damping (A&H-43)

is used together with the corrected equation for the scattering cross-section (A&H-56), it results in an inconsistent expression with A&H-55 (Ainslie and Leighton [2009]).

Calculated values of scattering cross-section of bubbles in harbour mud and ocean silt, normalized with respect to their geometrical cross sections, are plotted in Figs. 3.13 and 3.14, respectively. The current theory predicts a cross section almost two orders of magnitude higher for a bubble with radius approximately 1 mm in mud. It is interesting to note that A&H-55 agrees better with current formulation off-resonance, although A&H-56 was rather favoured by Anderson and Hampton.

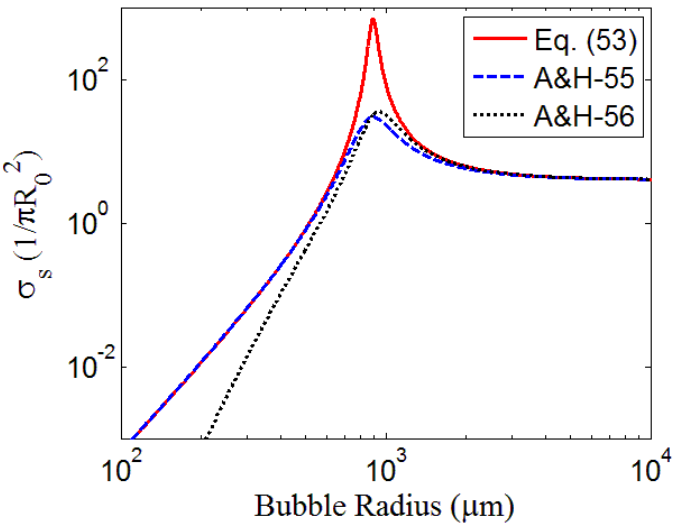

Figure 3.13: Scattering cross-sections for bubbles in harbour mud, driven by a 10 kHz pulse predicted by the current theory and A&H theory.

In Fig. 3.14, calculated values for the scattering cross-section of bubbles in ocean silt, driven by a 10 kHz are plotted. In contrast to the previous case, the current theory predicts a smaller value at the peak, resonant bubble radius. Similarly to the previous case, A&H-55 agrees better with current formulation for bubble radii less than its resonant value.

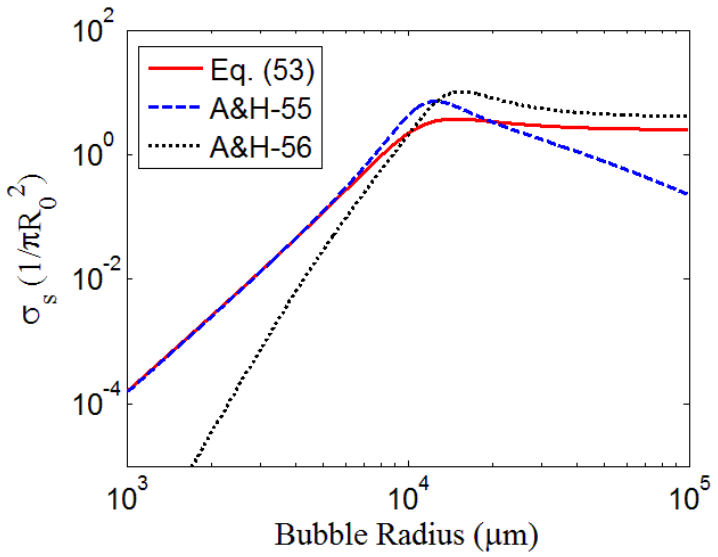

Figure 3.14: Scattering cross-sections for bubbles in ocean silt, driven by a 10 kHz pulse predicted by the current theory and A&H theory.

4 Discussions and conclusions

The commonly referred theory of Anderson and Hampton for the acoustic propagation in gas-bearing marine sediments involves semi-empirical expressions for the damping coefficients and some ambiguities with the speed of sound and scattering cross-section formulas. Further, some assumptions on linearity and mono-chromaticity limit its applicability in nonlinear time-dependent acoustic estimation models. Given the advances over few decades on the theory of both acoustics of gassy water and acoustics in a viscoelastic medium containing bubbles, a formulation which starts from fundamental physics principals, keeps the nonlinear time-dependent nature of the problem, and thus renders it applicable for more advanced acoustic estimation tools can be postulated and is presented in this report.

Both A&H theory and the current formulation agree on the fact that most effective dissipation mechanisms are the elastic, thermal and acoustic damping; where the former mainly depends on the bulk shear properties of the saturated sediment matrix, the thermal damping gets more significant when the driving frequency is low and the bubble radius is small, and the acoustic damping becomes more effective with increasing driving frequencies and larger bubble radius. For the expressions of damping coefficients, the two models significantly differ. For example, the thermal damping proposed by A&H, after multiplication by $\omega/2$ in order to match the dimensions, increases with increasing frequency whereas the

thermal damping modelled using the thermal viscosity decreases and the thermal damping given by Yang & Church (based on polytrophic relation) remains as constant with increasing frequency. Further, similarly after multiplication by ω/2, the elastic damping given by A&H decreases with increasing frequency whereas it is independent of the frequency in the current formulation. Among the most significant results, A&H theory predicts the elastic damping to be much higher (at least a few orders of magnitude) than other losses for all the cases studied here, for the given range of driving frequency and bubble radii.

For the scattering cross-section, the current formulation evaluates considerably higher values near the resonance regime for bubbles in harbour mud which is a fact consistent with observed lower values of damping and near resonance regime values of speed of sound. The case of ocean silt is somehow slightly different as three expressions, the current formulation with a correction owing to Ainslie and Leighton [2009, 2011], A&H-55 and A&H-56, produces different results for resonant bubbles and bubbles with larger radii than that. Nevertheless, for the given parameters the resonant bubble radius is 10 mm and it is unlikely to observe many bubbles with that size or larger.

References

Ainslie, M. A. and T. G. Leighton (2009), Near resonant bubble acoustic cross-section corrections, including examples from oceanography, volcanology, and biomedical ultrasound, *J. Acoust. Soc. Am., 126(5),* 2163-2175.

Ainslie, M. A. and T. G. Leighton (2011), Review of scattering and extinction cross-sections, damping coefficients, and resonance frequencies of a spherical gas bubble, *J. Acoust. Soc. Am., 130(5),* 3184-3208.

Anderson, A. L. and L. D. Hampton (1980a), Acoustics of gas-bearing sediment. I: Background, *J. Acoust. Soc. Am., 67(6),* 1865-1889.

Anderson, A. L. and L. D. Hampton (1980b), Acoustics of gas-bearing sediment. II: Measurements and models, *J. Acoust. Soc. Am., 67(6),* 1890-1905.

Best, A. I., Tuffin, M. D. J., Dix, J. K., and J. M. Bull (2004), Tidal height and frequency dependence of acoustic velocity and attenuation in shallow gassy marine sediments, *Journal of Geophysical Research*, 109, B08101.

Best, A. I., Richardson, M. D., Boudreau, B. P., Judd, A. G., Leifer, I., Lyons, A. P., Martens, C. S., Orange, D. L. and S.J. Wheeler (2006), Shallow Seabed Methane Gas Could Pose Coastal Hazard, *EOS Transactions, 87(22),* 213-217.

Caflisch, **R.E**., **Miksis, M.J., Papanicolaou, G.C. and L. Ting (1985)**, Effective equations for wave propagation in bubbly liquid, *Journal of Fluid Mechanics,153,* 259-273.

Church C. C. (1995), The effects of an elastic solid surface layer on the radial pulsations of gas bubbles, *J. Acoust. Soc. Am., 97(3),* 1510-1521.

Clarke, J.W.L. and T. G. Leighton (2000), A method for estimating time-dependent acoustic cross-sections of bubbles and bubble clouds prior to the steady state, *J. Acoust. Soc. Am., 107(4),* 1922-1929.

Kamath, V. and A. Prosperetti (1989), Numerical integration methods for gas-bubble dynamics, *J. Acoust. Soc. Am., 85(4),* 1538-1548.

Landau L. D. and E. M. Lifshitz (1958), Fluid Mechanics, *Pergamon*, Oxford, Chap. II

Leighton, T.G., Meers, S.D. and P. R. White (2004), Propagation through nonlinear time-dependent bubble clouds and the estimation of bubble populations from measured acoustic characteristics, *Proc. R. Soc. Lond. A, 460(2049),* 2521-2550.

Leighton, T. G. (2007), Theory for acoustic propagation in marine sediment containing gas bubbles which may pulsate in a non-stationary nonlinear model, *Geophysical Research Letters, 34,* L17607.

Lyons A. P., Duncan, M. E. and A. L. Anderson (1996), Predictions of the acoustic scattering response of free-methane bubbles in muddy sediments, *J. Acoust. Soc. Am., 99(1),* 163-172.

Prosperetti, A., and A. Lezzi (1986), Bubble dynamics in a compressible liquid. Part 1. First-order theory, *Journal of Fluid Mechanics,168,* 457-478.

Prosperetti, A., Crum, L. and K. W. Commander (1988), Nonlinear bubble dynamics, *J. Acoust. Soc. Am., 83,* 502-514.

Spitzer, L. Jr. (1943), Acoustic properties of a gas bubble in a liquid, *OSRD Report 1705* (Division of War Research, Columbia University)

Storey, B. D. and A. J. Szeri (2001), A reduced model for cavitation physics for use in sonochemistry, *Proc. R. Soc. Lond. A,* 457, 1685-1700.

Stricker, L., Prosperetti, A. and D. Lohse (2011), Validation of an approximate model for the thermal behavior in acoustically driven bubbles, *J. Acous. Soc. Am.* , 130(5), Pt. 2, 3243-3251.

Yang, X. and C. C. Church (2004), A model for the dynamics of gas bubbles in soft tissue, *J. Acoust. Soc. Am., 118(6),* 3595-3606.